

Chapter 4

Thermomechanical Analysis in Welding



Abstract Mechanical analysis of welded joint is performed to calculate the residual stress and distortion generated during the welding process and cooling. Thermal elastic–plastic FEM analysis for doing so is usually performed using static implicit or quasi-static explicit methods. The strategies which can be employed to reduce the calculation time are described in this chapter. It is also explained how a mechanical analysis can be performed in a large-scale structure using approaches such as the inherent strain method. The effect of phase transformation in mechanical analysis is also discussed. Considering plasticization behavior of material and phenomena such as creep and annealing on mechanical analysis can increase the accuracy of simulation and in this chapter it is explained how one can implement these considerations in mechanical analysis. Finally, the effect of these phenomena on residual stress during welding are also addressed.

4.1 Residual Stress and Distortion

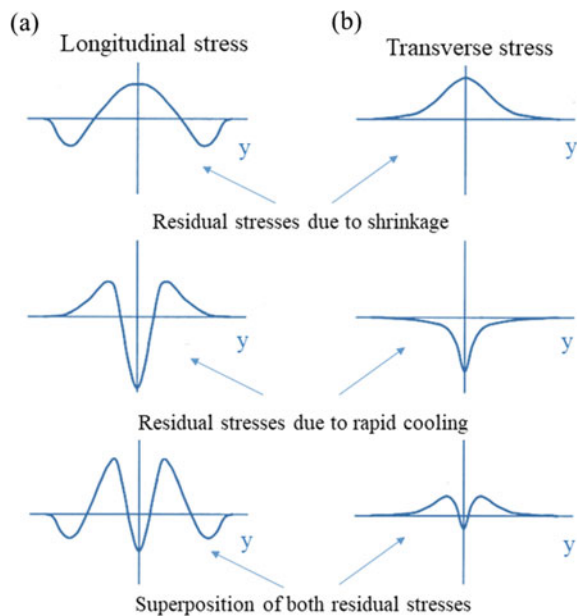
Residual stresses are, by definition, internal stresses and are mechanically in equilibrium and are formed without any applied external load. Knowledge about the type, amount, and distribution of residual stresses can help to predict structure performance under various loading conditions. During loading, residual stresses can influence the failure of the structure especially when they are aligned with the applied loads. Residual stresses can also influence stress corrosion cracking [1], cold cracking [2] and fatigue strength [3]. The residual stresses raised during welding are commonly termed as “welding residual stresses” and are formed due to a heterogenous plastic deformation field, which is caused by a local thermal source used in the welding process [4]. The existence of plastic deformation in every location is incompatible with its surroundings and occurs at the macroscopic, microscopic and submicroscopic levels in the weld, HAZ, and base material [5]. Residual stresses, when aligned in the loading direction, cause earlier plasticization and reduction of the local strength.

Residual stresses can be classified into four main groups:

1. Thermal, which are developed during cooling through differential deformation in the cross section, resulting from thermal expansion;
2. Deformation, which result from an inhomogeneous plastic deformation field from an external loading;
3. Phase transformation, caused by uneven phase transformation and a volume change;
4. Precipitation, a distortion stemming from the occurrence of precipitation in the crystal structure.

The sources of residual stresses in the welding region are shrinkage, rapid cooling and phase transformation [6]. Residual stresses due to shrinkage are always tensile in both transverse and longitudinal directions. To establish the equilibrium in a transverse direction, the compressive residual stresses are formed away from the weld in the HAZ and the base material. The mechanisms that underly the formation of residual stresses due to rapid cooling are similar to those formed due to shrinkage, occurring when the cooling rate is high enough to cause a large temperature gradient and severe constraints. In the thickness direction of thin sheets, in which the temperature distribution is uniform, this kind of residual stresses do not exist. The temperature around the weld zone is lower and therefore serves as a constraint in longitudinal direction. Perpendicularly to the weld, the boundary condition of the weld and the material of the weld both determine the residual stress [7]. In addition to the material, thickness and boundary conditions, the welding process and its parameters influence the residual stress. Figure 4.1 shows the residual stresses caused by shrinkage and

Fig. 4.1 Development of **a** longitudinal, and **b** transverse residual stresses due to shrinkage and rapid cooling and their superimposition along the longitudinal direction (x-direction) and the transverse direction (y-direction) for an Al–Si–Mg alloy [8]



rapid cooling and their superimposition in both longitudinal and transverse directions for an Al-Si-Mg alloy [8].

A structure with large global stiffness is highly constrained. When the edge of the weld has no constraint, the composition of the weld is important in determination of the perpendicular residual stress [7]. In general, single-layer welds without an edge constraint develop lower residual stresses in the transverse direction. Hindered longitudinal shrinkage due to reaction forces leads to the reduction of the plastic deformation and develop residual stresses in the direction of the weld. The forces caused by the residual stresses in the structure are in balance and therefore the tension in the middle of the weld seam is balanced by compression at the end of the weld seam. Transversely to the weld seam, the residual stresses due to shrinkage reduce from the center to the edges. Generally, residual stresses in the thickness direction arise from different cooling rates along the thickness and are mostly formed in sufficiently thick sheets or in multilayer welding.

The determination of residual stress via numerical simulation requires a thermal analysis, used to first calculate the spatial and temporal temperature distribution and then coupled with a mechanical analysis to calculate the resulting stresses. Distortions are usually coupled with residual stresses and occur in the longitudinal, transverse and angular directions or any combination of these [5]. In general, a FEM simulation for mechanical analysis requires a set of governing equation, the concepts of which are described below.

A change in temperature in a metal bar is always associated with a change in its length, which is dependent on the modulus of elasticity. Any increase in temperature causes the interatomic distance to increase which is equivalent to a change in the lattice parameter. The elastic strain (ε_{el}) is related to the lattice spacing change according to the following equation:

$$\varepsilon_{el} = \frac{d - d_0}{d_0} \quad (4.1)$$

where d is the lattice spacing of the specimen when is under stress and d_0 is the lattice spacing of the specimen when it is free of stress. This elastic strain is proportional to the temperature change according to the following equation:

$$\varepsilon_{el} = \alpha \Delta T \quad (4.2)$$

where α is the coefficient of thermal expansion, which can be temperature dependent. If a metal is heated evenly and no constraint exists in the way of expansion, the atomic distance increases without inducing any interaction load. However, in the presence of constrains, residual stresses arise during the expansion and contraction of the material. As mentioned before, the constraints can be mechanical in nature or can result from uneven heating. Uneven heating is the main mechanism behind the development of residual stresses during a welding process, and any mechanical constraints can enhance this effect. In most cases, there is an interest to calculate the residual stresses after cooling. The origin of these stresses is the plastic strain that

occurs when the elastic limit of the material is exceeded. The plastic yielding occurs when:

$$f = \sqrt{\frac{3}{2} \cdot \{S_{ij}\}^T \cdot \{S_{ij}\}} - \sigma_f = 0 \quad (4.3)$$

where s_{ij} is the deviatoric stress and σ_f is the yield stress. The local yield point itself depends on the local temperature and the yield point of metals and alloys decreases with increasing temperature. The numerical FE simulation offers the possibility to take into account the variation of the yield strength with the temperature and to increase the accuracy of the mechanical models. The residual stresses in each spatial direction ($\sigma_{res,i}$) are related to the elastic strain according to Hooke's law:

$$\sigma_{res,i} = \frac{E}{1 + \nu} \varepsilon_i + \frac{\nu E}{(1 + \nu)(1 - 2\nu)} (\varepsilon_x + \varepsilon_y + \varepsilon_z) \quad (4.4)$$

where E is the elastic modulus, ν is the Poisson coefficient, and ε_i is the strain in the direction of i . the elastic modulus is also temperature-dependent and decreases with increasing the temperature.

Phase transformations during cooling and heating can also contribute to the development of residual stresses, since they induce strains, namely phase transformation strains. In fusion welding processes, there is an increase in volume due to melting and, conversely, when solidifying. This type of phase transition has no effect on the residual stress development since both melting and solidification take place at high temperatures where the tensile stress is almost zero. The yield point is only significant below a certain temperature and can promote the residual stresses. Thus, one can neglect the melting and solidification processes as well as any phase transformation that occurs at high temperatures, since the yield strength is low at high temperatures and no residual elastic strain can be induced. For this reason, only the phase transitions that take place at lower temperatures should be considered in a mechanical analysis.

4.2 Numerical Simulation for Mechanical Analysis

The main outputs of the mechanical analysis are deformation and geometry variations as well as the stress and plastic strain distribution. There are two main approaches to calculate residual stress during welding. In the decoupled thermomechanical analysis, an FE heat transfer analysis is carried out first, which can also include the phase change analysis. Then, a separate FE thermal-stress analysis will be performed which is based on continuum mechanics and only calculates the macro residual stress [9]. This decoupling has a negligible influence on the simulation accuracy, since the mechanical state of the material has minimal influence on the thermal properties and the phase transformation [5]. An alternative approach performs both thermal

and mechanical calculations at the same time which is referred to as coupled thermo-mechanical analysis. In a coupled transient thermal static structural analysis, the heat transfer problem is solved first, with the temperature history being saved for each node. Then, structural nodal loads are calculated using the thermal expansion coefficient in static conditions through the nodal temperature history. The coupled models assume that thermal energy and mechanical energy are equivalent and thus these analyses start with the fundamental equation of thermo-mechanics [10]:

$$cq\dot{T} + \dot{q}_{i,i} = \dot{Q}_v - \frac{E\alpha T}{1-2\nu}\dot{\varepsilon}_{eii} + \xi\sigma_{dij}\dot{\varepsilon}_{vpij} \quad (4.5)$$

where $cq\dot{T}$ is the heat stored energy per unit of time, $\dot{q}_{i,i}$ is the heat supplied or carried away (through surface), \dot{Q}_v is the heat released or consumed per unit of time (related to volume), $\frac{E\alpha T}{1-2\nu}\dot{\varepsilon}_{eii}$ is the energy released from elastic deformation and $\xi\sigma_{dij}\dot{\varepsilon}_{vpij}$ is the energy due to viscoplastic deformation. A part of the energy used for plastic deformation is stored as microstructural changes and therefore a factor of ξ is used to state how much of this energy is converted to heat. This factor, in most cases, is close to 1 showing that almost all the energy for plastic deformation is converted towards heat. Coupling between thermal and mechanical fields can be ignored in welding as the heat is supplied solely from an outside source.

In a decoupled thermo mechanical analysis, two models, thermal and mechanical, are solved separately and sequentially. Usually, the mechanical analysis consumes more resources than the thermal analysis, due to the higher degree of freedom of the problem to be solved [11]. The stress distribution is calculated using FE methods, following the known strain components. Prior to each mechanical modelling step, the temperature distribution obtained from thermal analysis is loaded as a predefined field and the material properties of each node are suitably updated. Thermo-elastic-plastic (TEP) material behavior is described by the method of incremental strain change [12], where the total strain is obtained from [5, 12]:

$$\varepsilon = \varepsilon_{in} + \varepsilon_{el} + \varepsilon_{pl} + \varepsilon_{th} + \varepsilon_{tr} + \varepsilon_{tp} + \varepsilon_{cr} \quad (4.6)$$

In which ε_{in} , ε_{el} , ε_{pl} , ε_{th} , ε_{tr} , ε_{tp} , and ε_{cr} are initial, elastic, plastic, thermal, transformation, plastic, and creep strains, respectively. For an isotropic material with an elastic modulus of E , a Poissons ratio of ν , shear modulus of G , the strain in 3D in the elastic region (ε_{el}) is obtained from:

$$\varepsilon_{el} = [D]^{-1} \cdot \sigma \quad (4.7)$$

where $[D]$ is the stiffness matrix. The plastic strain is derived from:

$$d\varepsilon_{pl} = \lambda_p \cdot \frac{\partial f}{\partial \sigma} \quad (4.8)$$

where λ_p is a multiplier dependent on the problem and f is obtained from Eq. 4.2. The thermal strain is obtained from:

$$\varepsilon_{th} = \alpha(T) \cdot (T - T_0) \quad (4.9)$$

where $\alpha(T)$ is the thermal expansion coefficient which is dependent to temperature, T is the temperature and T_0 is the reference temperature. For the stress and strain field simulation, it is essential to determine the dependency of Poisson's ratio, Young's modulus, thermal expansion coefficient, and yield limit to the temperature [13]. There are two numerical approaches suitable to solve the mechanical models; static implicit and quasi-static explicit. In the following paragraphs, these two approaches are described in more detail.

4.2.1 Implicit Approach

The numerical simulation for mechanical modeling can be carried out in the static as well as in the dynamic states. In the static approach, no inertia effects are taken into account and only the load equilibrium is solved. A static approach for solving a mechanical model is applicable when the load frequency is less than $\frac{1}{4}$ of the natural frequency, so no inertia effects are present. In this way, the kinetic energy would be zero and the dynamic approaches (implicit dynamic and explicit dynamic) would give the same result as static approach. The dynamic approaches are mostly used when the inertia effect is not negligible but in the simulation of welding problems, the static approach is usually sufficient since inertia plays a minor role in the process. In a static analysis, when there are moving objects or an imposed displacement, it is important to properly define the constraints and limit the degree of freedom (DOF), otherwise the solving procedure will not converge.

For solving large-scale welding deformation problems using an implicit FEM analysis, the memory usage is high because there is a high order relationship between the arithmetic operations and the number of degrees of freedom [14]. Software packages such as JWRIAN [15] and SYSWELD are mostly based on an implicit method. The general equation for the static implicit FEM used in this process is:

$$K \cdot \Delta U = \Delta F \quad (4.10)$$

where K is the stiffness matrix, ΔU is the increment of displacement and ΔF is the load increment. ΔF consists of both external load and thermal load. When 'n' nodes exist, the implementation of this equation in elastic region yields the following matrix:

Table 4.1 Velocity scaling method used in implicit approach [16]

Variable (unit)	Scaled value (ξ : Scale factor)
T (s)	t/ξ
Δt (s)	dt/ξ
v (mm/s)	ξv
\dot{Q} (J/mm ³ s)	$\xi \dot{Q}$
\dot{q} (J/mm ² s)	$\xi \dot{q}$
λ (J/mm s°C)	$\xi \lambda$
β (J/mm ² s°C)	$\xi \beta$
C (J/kg°C)	C
ρ (kg/mm ³)	ρ

$$\begin{bmatrix} k & \cdots \\ \vdots & \ddots & \vdots \\ \cdots & k \end{bmatrix} \begin{Bmatrix} \Delta u_1 \\ \vdots \\ \Delta u_{3n} \end{Bmatrix} = \begin{Bmatrix} \Delta f_1 \\ \vdots \\ \Delta f_{3n} \end{Bmatrix} \quad (4.11)$$

There are $3n$ possible displacements as every node can move in 3 directions. ‘K’ is the quasi-zero components of the stiffness matrix. The number of these components is proportional to n^2 . The time increment used in an implicit analysis is determined by temperature increment. When an implicit analysis is used for heat conduction analysis, a velocity scaling factor can be used to shorten the analysis time. Accordingly, the heat flow rate and the materials characteristics related to time are scaled by a factor of ξ . Table 4.1 shows the values obtained by velocity scaling of specified physical quantities.

In a static implicit FEM used for welding mechanical analysis, several steps should be defined for applying the loads. A global stiffness equation should be solved for each load step which a very memory-intensive step for large-scale structures and with long computational times [17]. Welding problems possess high non-linearity especially around the weld line and the process of solving this non-linearity should be performed by iterative calculations such as Newton–Raphson method. The stiffness matrix of the whole structure is updated for each increment which is very time-consuming. Thus, an iterative substructure method (ISM) is often used to avoid frequent updating of the global stiffness matrix [11, 14]. With this method, the area near the moving heat source, which has a strong non-linearity, is solved separately from the remaining region (Region ‘B’ in Fig. 4.2a). The remaining region (region A-B in Fig. 4.2a) behaves elastically and an elastic stiffness matrix is assigned to the whole structure (K_A^e) initially, with its inverse being saved. The stiffness matrix of the nonlinear region (K_B^n) is updated in every temperature increment while the remaining region (A-B) is only solved and updated every N_{A-B} increment using the initially saved inverse matrix of K_A^e . Since the stiffness matrix is only updated incrementally for region ‘B’, the computational time can be shortened. The continuity of the displacement at the interface of the two regions can be directly maintained and

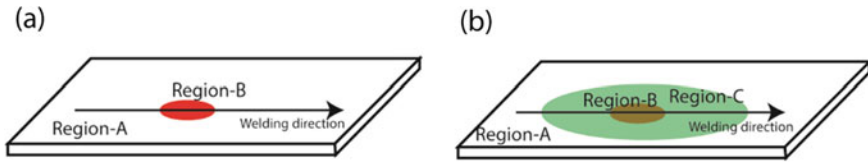


Fig. 4.2 Computation of stiffness and stress in **a** ISM method, and **b** i-ISM method

the continuity of the traction is maintained by the iterative correction process. For larger components, defined as those that consist of more than 1 million elements, one can introduce even more regions in order to shorten the calculation time (Fig. 4.2b). In this way, region C-B is treated like the region A-B in the previous example. Therefore, region A-C requires a lower number of stiffness matrix updates by a factor of $1/N_C$, in which N_C is the number of steps needed to update the stiffness matrix of region C-B. This method is named the inherent strain ISM (i-ISM) method. In the following paragraphs, it is described how the ISM method can be implemented during welding by a moving heat source.

As mentioned, in ISM one area around the welding zone exhibits strong nonlinear behavior while the remaining areas exhibit linear behavior or a small stiffness change (quasi-linear). Figure 4.3.a shows how the stiffness matrix is updated when the heat source is moving. The non-linear region moves as the torch moves and the non-linear region thus changes from 'B' to 'B'' and the stiffness matrix is updated to nonlinear, while the stiffness matrix of the remaining region remains linear. The continuity at the boundary of these two regions should be maintained in the iterations. The stiffness matrix of region A' + B' can be maintained over the process as long as there is convergence in the solution and the initial stiffness matrix can be used until the end of the process. This reduces the calculation time considerably. The schematic of the procedure used to calculate the stress is shown in Fig. 4.3b. The stress is obtained by considering the continuity and balance of stress at the boundary. It is important to define the border between the linear and non-linear regions properly. Underestimating the extent of the non-linear region will compromise the accuracy of the results, although the computational time will decrease. The extent of the nonlinear area can be defined as a distance over which the accuracy of the results does not change (is not improved) and this area can be defined as a region whose maximum temperature is greater than a specified one. In this area, the temperature gradient is steep, and the local yield point is low enough to induce local plastic strains and residual stresses. The mesh size in the linear region is set to be coarser since it is linear in nature.

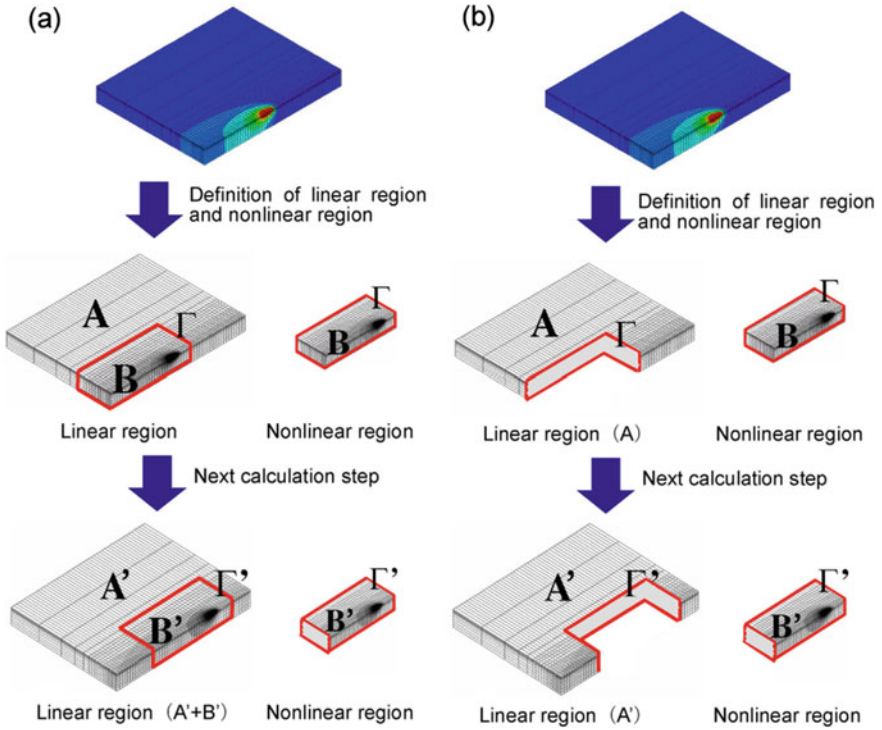


Fig. 4.3 Region division in the iterative substructure method for **a** constituting the stiffness matrix, and **b** stress calculation [18]. Reprinted with permission from Elsevier

4.2.2 Explicit Approach

The explicit method is suitable for modelling dynamic phenomena which take place in a short period of time [16]. However, it can be adapted for mechanical analysis of welding which in this case is named as a quasi-static explicit method. In explicit method, the time increment (time step) should be selected in a way to ensure that the stress wave propagation distance is smaller than the element size. The basic equation of dynamic explicit FEM is [17]:

$$[M]\{\ddot{U}\}_t + [C]\{\dot{U}\}_t + \sum_{e=1}^{Ne} \int [B]^T \{\sigma\} dV = \{F\}_t \quad (4.12)$$

where $[M]$, $[C]$, $[B]$, and $\{\sigma\}$ are the mass matrix, damping matrix, strain–displacement matrix and stress vector, respectively. $\{\ddot{U}\}_t$, $\{\dot{U}\}_t$, and $\{F\}_t$ are acceleration, velocity, and load vector at time t . Ne is the number of elements and dV is the volume of each element. In the simulation of welding, the scale of simulation is usually limited to the welding joint area. Idealized Explicit Finite Element Method

(IEFEM) can be used to perform simulations in larger scales [17]. In this method, the load is applied in several increments and the displacement in every increment is calculated based on the above equation until the static equilibrium state is reached in that load increment. Thereafter, a new load increment is applied and the procedure is repeated. For large scale problems, the amount of memory needed for an explicit analysis is generally less than that necessary for an implicit one [16], since in the explicit method, there is no need to perform convergence calculations. The time increment in the explicit analysis should then be:

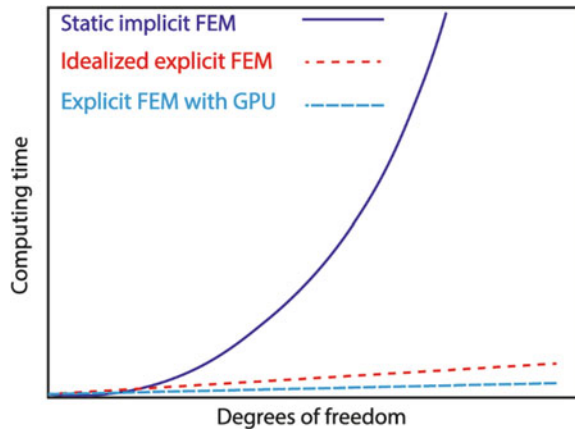
$$\Delta t < L/c \quad (4.13)$$

where ‘L’ is the minimum size of an element and ‘c’ is the wave propagation speed which is obtained from:

$$c = \sqrt{\frac{E(1 - \nu)}{\rho(1 + \nu)(1 - 2\nu)}} \quad (4.14)$$

Some methods such as mass scaling, are commonly used to shorten the calculation time in an explicit analysis. By scaling the mass, ‘c’ is virtually reduced and therefore the step time is increased. The elastic modulus and Poisson ratio should not be changed because these parameters directly affect the calculation of the stiffness and stresses acting on the material. However, using mass scaling causes a degree of dynamic vibration which can be eliminated by considering a damping coefficient between 20–100% of the minimum angular frequency in the analysis [16]. By using an explicit method we can take the advantage of using several CPU or Graphic Processing Unit (GPU) cores in parallel, as the explicit equations can be solved independently for each node [14]. This parallelization can take the advantage of GPU to accelerate the computation time in explicit method. Figure 4.4 shows a comparison between the two approaches, static implicit and explicit (idealized and

Fig. 4.4 Comparison between the two approaches, static implicit and explicit (idealized and using GPU) in terms of calculation time [17]. Adopted with permission from Elsevier



using GPU) in terms of calculation time. In a static implicit approach, the stiffness matrix is updated in each increment and, depending on the DOF of movement of each element, several elements of the stiffness matrix must be calculated and updated. In the explicit method, the mass matrix is updated in each increment which is a diagonal matrix and a reduced number of elements need to be updated. Hence, for a large structure an explicit analysis requires a lower calculation time.

Velocity scaling is another commonly used technique to reduce calculation time in a FEM explicit deformation analysis performed for quasi-static condition. In this method, strain velocity is accelerated. The temperature change rate can also be accelerated to decrease the calculation time. By using velocity scaling in a thermal elastic–plastic analysis, the mechanical characteristics of materials such as Young’s modulus E , Poisson’s ratio ν , yield stress s , work-hardening coefficient H and thermal linear expansion coefficient cannot be scaled.

4.3 Thermal Elastic–Plastic FEM for Small Scale Structures

The thermal elastic–plastic (TEP) method can yield both the temperature and stress fields and is mostly suitable for analysis of small structures, since it is computational heavy [13]. In this way, the weld is considered as a transient nonlinear problem. Figure 4.5 shows the steps needed in the thermo elastic–plastic FEM analysis to determine the residual stress and deformation [19]. Small structures, which typically consist of a single weld line, can be analysed using this method. For larger structures, which are made up of multiple components connected by several weld lines,

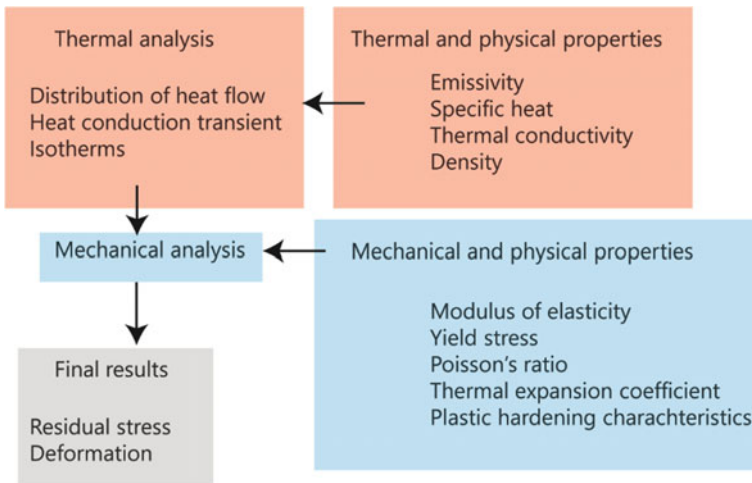


Fig. 4.5 The flowchart of TEP FEM

TEP analysis leads to computational times which are much higher and therefore this method is unpractical for these applications and rarely used in full structures. In those more complex cases, weld lines are first classified based on their geometry, dimension, and welding process. Instead of analysing all the weld lines simultaneously, only each classification will be analysed by the TEP method. Thereafter, the results of the TEP analysis are used as input for other approaches that are more efficient and thus can be used to perform a mechanical analysis of the entire structure. Two of these approaches are discussed in the next two subsections.

Before it can be used, a TEP analysis needs to be calibrated and validated experimentally. When TEP is used on a small yet complex structure, the validation of the analysis can be performed on a simplified specimen, dispensing tests on the real structure, since the real structure often consist of components that may have been prefabricated by complex processes. Figure 4.6 (left) shows the results of a calibrated model for prediction of distortion verified by experiment on a simple lap joint. In Fig. 4.6 (right) a real structure is shown, which is complex and simulated by the calibrated model to predict the distortion level. No experiment is performed to validate this result.

In a TEP FEM it is fundamental to consider the interaction of the materials properties with both the thermal and mechanical models [21], as shown in Fig. 4.7. The consideration of both physical and mechanical properties and their temperature dependency during the simulation can be decisive in the thermal and mechanical analysis. The effect of material properties will be discussed later in this chapter.

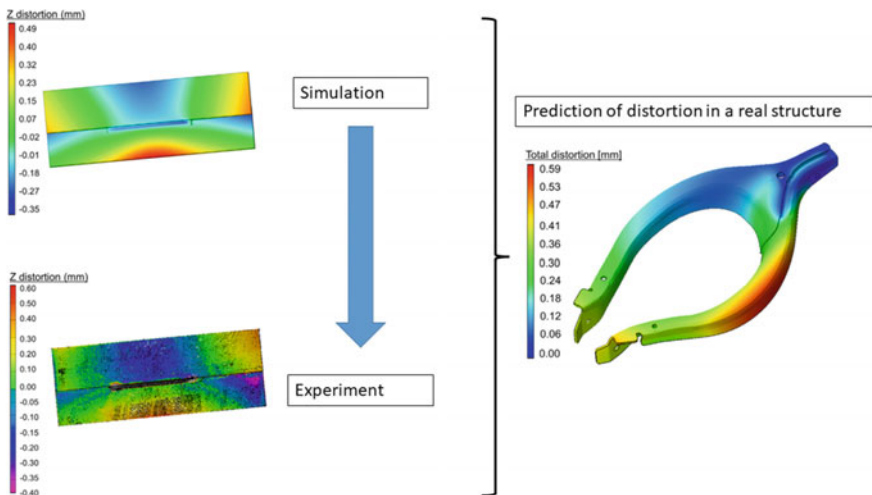


Fig. 4.6 (Left) The results of a calibrated model for prediction of distortion verified by experiment on a simple lap joint. (Right) The real structure which is complex and is simulated using the calibrated model to predict the distortion. The color map shows the distortion [20]. Adopted with permission from Elsevier

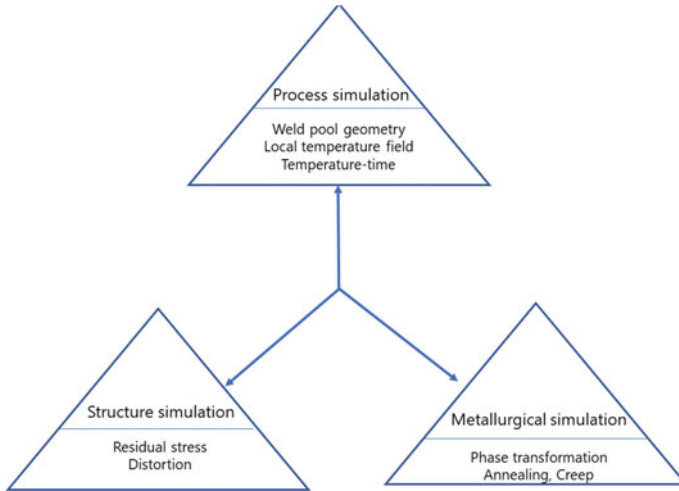


Fig. 4.7 Interaction of the materials properties with both thermal and mechanical models

4.4 Inherent Strain Method

As previously stated, if one wishes to calculate the residual stress and the distortion in a large and complex structure the use of TEP-FEM as the sole method is highly discouraged, since it is an extremely resource heavy and time-consuming process. An alternative approach for the determination of the distortion and residual stress for large and complex structures consists in the use of the inherent strain method. In this way, a TEP-FEM and a linear FEM analysis are used to calculate the residual stress and distortion [22]. The linear FEM analysis uses an inherent strain as initial strain. The inherent strain is obtained by using TEP-FEM method for each weld line and this considerably reduces the calculation time. In the linear analysis, the structure can be fully represented by shells, which further shortens the calculation time [13]. The level of this inherent strain is dependent on the peak temperature and the existing constraints [23]. In this approach, the inherent strain values calculated by TEP FEM simulation for each individual weld are used as an initial load in the mechanical linear FEM simulation in a global shell, allowing to calculate the distortion in large and complex structure [24]. Therefore, the time needed for calculation is drastically decreased, as the non-linear TEP FEM model does not need to be applied to the whole structure. This procedure is shown schematically in Fig. 4.8 [25].

The inherent strain calculated by TEP-FEM analysis is converted to either force or deformation for use in a linear FEM analysis. When a strong constraint exists, the inherent strain is transformed to stress and when there is a small restraint the inherent strain is transformed to deformation [22]. In the linear FEM model for calculation of transverse shrinkage and bending (angular distortion) the inherent deformation can be used when the restraints in transverse direction are negligible. For longitudinal shrinkage and bending, the inherent force or moment can be used for linear FEM

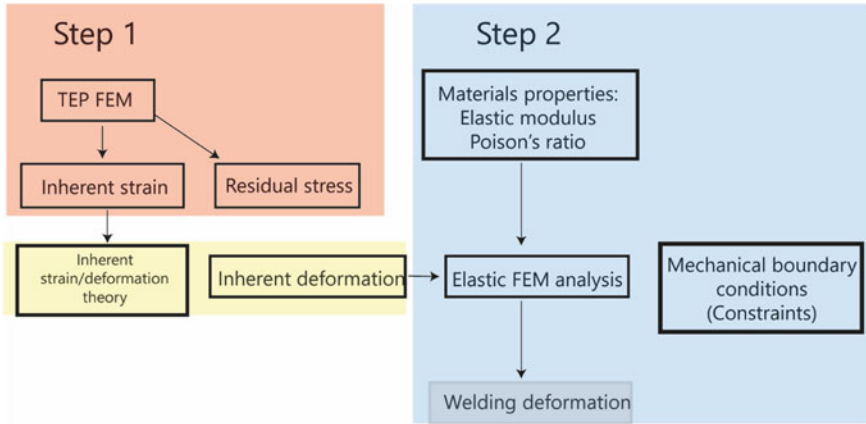


Fig. 4.8 The flowchart of calculation of inherent strain by TEP FEM (step 1) and using it in the subsequent linear FEM (step 2)

modelling, as the restraint in longitudinal direction is huge. Figure 4.9 shows the transverse shrinkage (δ_y^*) as well as the longitudinal force (F_L^*) resultant from the longitudinal shrinkage calculated using the inherent strain components (ϵ_x^* and ϵ_y^*). Shrinkage in one direction is always associated with shrinkage in the other direction, and these two are linked by Hooke's law. Figure 4.9c and d show both mentioned deformation and force in an element.

These concepts can be integrated into a FEM model, allowing to predict the residual stress and distortion [22]. The inherent strain is obtained from the following equation:

$$\epsilon^* = \epsilon - \epsilon^e = \epsilon^p + \epsilon^{th} + \epsilon^{cr} + \epsilon^{tr} \quad (4.15)$$

ϵ^p , ϵ^{th} , ϵ^{cr} , and ϵ^{tr} are plastic strain, thermal strain, creep strain, and transformation strain, respectively. ϵ^* is considered as the inherent strain which contributes to the welding deformation. The inherent strain can be schematically explained as depicted in Fig. 4.10. When a material is stressed, a strain is induced and when a piece of the material is cut, one part of the strain is released which is elastic and associated to the residual stress. The component of strain that is irrecoverable after cutting is referred to as an inherent strain [27].

The inherent strain can also be obtained experimentally. When using the simulation results obtained by TEP FEM, it is important to verify those results with some experiments. The inherent strain values are uniform along the weld line except the beginning and the end of the joint. It is because the thermal condition at the beginning and the end of the joint is not quasi-static. In addition, the restraints at the beginning and at the end of the weld are different from those in the rest of the weld line.

The inherent strains are usually calculated in the transverse direction and in some cases in the longitudinal direction [24]. The deformations caused by inherent strain

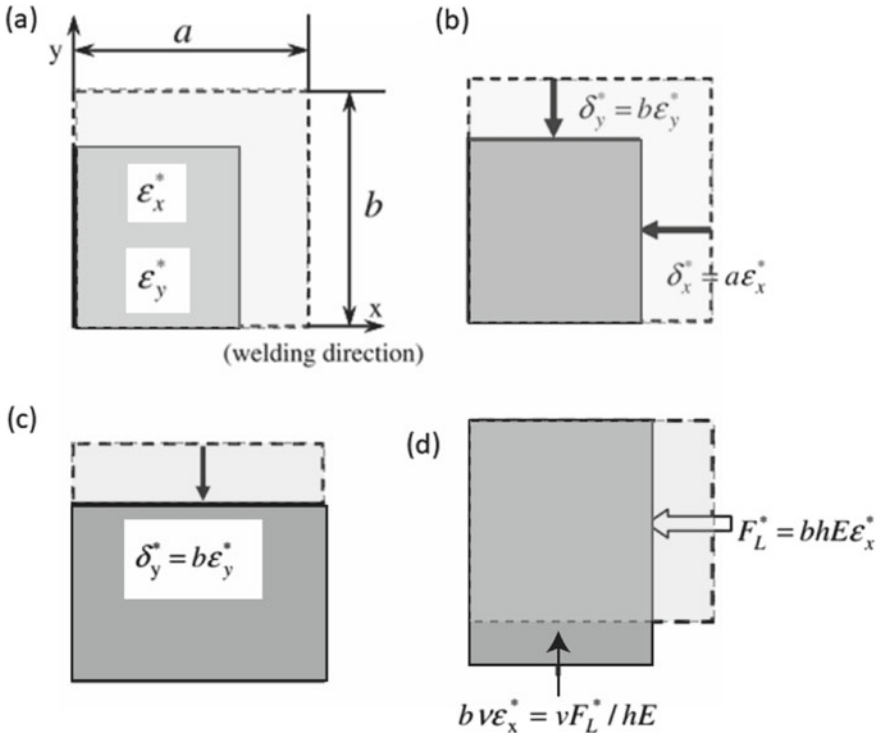


Fig. 4.9 **a** Shrinkages represented by inrent strain. **b** Shrinkage represented by inherent deformation. **c** Transverse shrinkage. **d** Longitudinal shrinkage [26]. Adopted with permission from Elsevier

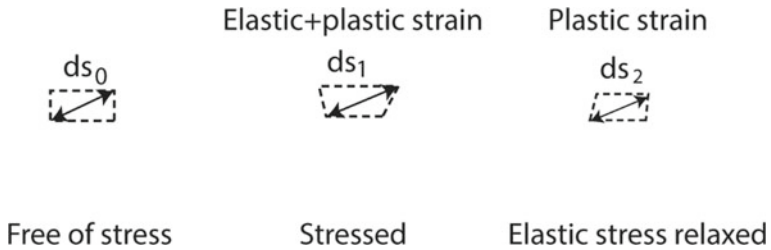
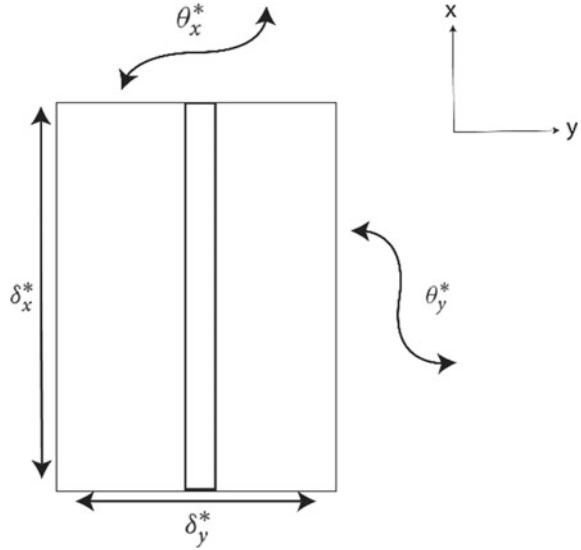


Fig. 4.10 Definition of inherent strain (ds_2) as the plastic strain in a stressed body

values are averaged through the thickness (z), perpendiculary to the weld direction (y -direction) according to the following equations [22]:

$$\delta_x^* = \frac{1}{h} \int \int \epsilon_x^* dy dz \tag{4.16}$$

Fig. 4.11 Schematic of shrinkage and bending resulted from inherent strains in transverse and longitudinal directions



$$\delta_y^* = \frac{1}{h} \int \int \varepsilon_y^* dy dz \quad (4.17)$$

$$\theta_y^* = \frac{12}{h^3} \int \int \left(z - \frac{h}{2} \right) \varepsilon_y^* dy dz \quad (4.18)$$

$$\theta_x^* = \frac{12}{h^3} \int \int \left(z - \frac{h}{2} \right) \varepsilon_x^* dy dz \quad (4.19)$$

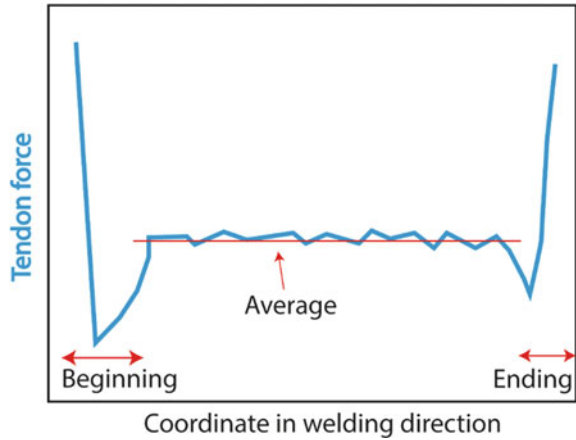
δ_x^* and δ_y^* are the inherent deformation in x and y directions, respectively. θ_x^* and θ_y^* are the inherent bending in x and y directions, respectively (Fig. 4.11). 'h' is the thickness of the welded structure.

Longitudinal shrinkage is represented by Tendon force (F_T) which is obtained from:

$$F_T = E \int \int \varepsilon_x^* dy dz = Eh\delta_L^* \quad (4.20)$$

This force is the driving force for buckling in thin plates whose resistance to buckling is low. The value of Tendon force in the beginning and in the end of the weld is different from the rest due to the free restraint effect. An average of this force along the longitudinal direction is calculated, disregarding the end and beginning, as shown in Fig. 4.12 [28]. This average value accounts for the total Tendon force that will be used as an inherent force in linear FEM model. In the linear FEM model, the longitudinal shrinkage, the transverse shrinkage, and the angular distortion are used as initial strains. Instead of the longitudinal shrinkage, the Tendon force can be used to represent the longitudinal shrinkage. When transferring the results

Fig. 4.12 Distribution of tendon force along the longitudinal direction of the weld



obtained from TEP FEM analysis into the global model, it is important to choose the right boundary conditions and welding sequences. Away from the weld zone the inherent strain is equal to the plastic strain, since the thermal strain and the phase transformation induced strain are negligible [29]. In the linear FEM analysis, the inherent deformation components are employed as mechanical loads (displacements) [25].

The inherent strains can also be measured by experimental methods such as cutting procedure [29]. In this way, the residual stress as well as the deformation in the structured can be calculated using the experimentally measured inherent strains. The basic equations of the linear FEM model are [29]:

$$[K]\{u\} = \{f^*\} \tag{4.21}$$

$$\{f^*\} = \int [B][D]\{\varepsilon^*\}dv \tag{4.22}$$

where $[K]$, $\{u\}$, and $\{f^*\}$ are the elastic stiffness matrix, the nodal displacement and the inherent strain induced nodal force. dv is the volume of element and $[B]$ is the corresponding matrix between the nodal displacement and strain in an element. The displacement field obtained from the above equations will be used in the following equations to calculate the total strain ($\{\varepsilon\}$) and the residual stress ($\{\sigma\}$):

$$\{\varepsilon\} = [B]\{u\} \tag{4.23}$$

$$\{\sigma\} = [D^e](\{\varepsilon\} - \{\varepsilon^*\}) \tag{4.24}$$

where $[D^e]$ is the material elastic matrix.

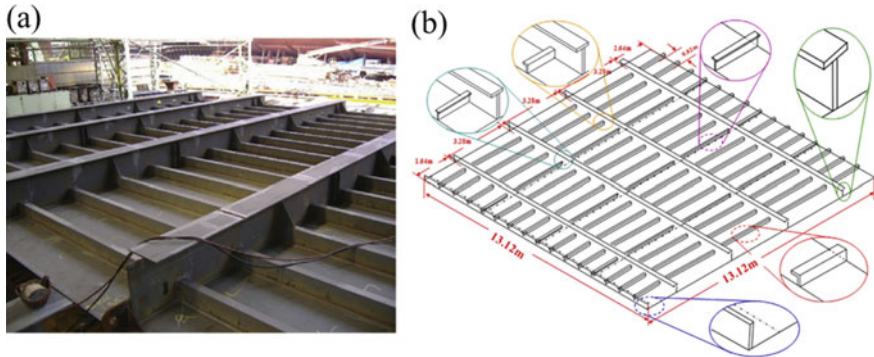


Fig. 4.13 **a** Plates and stiffeners of a ship panel structure. **b** The categorized weld lines in the panel [25]. Reprinted with permission from Elsevier

The inherent strain calculated using the TEP-FEM method is mainly used for deformation analysis by linear FEM. Figure 4.13a shows a car deck panel structure used in a large ship. It consists of plates and stiffeners which are welded together. Please note, however, that the welding conditions are different for different joints of the structure. Figure 4.13b shows that the welds can be categorized into six main groups. In this example, in order to determine the buckling of the structure during welding, a TEP-FEM analysis was first carried out for each type of weld in order to obtain the inherent strain. The simulation results for each category of weld were verified experimentally. The inherent strains obtained from this TEP FEM model were used in an elastic FEM model to measure the distortion by both small deformation theory and large deformation theory. Buckling of the structure was calculated without considering the bending in both directions and only transverse and longitudinal shrinkage were used for doing so.

When assembling the parts for the linear FEM analysis, it is necessary to position each part so that it is initially free to move, and a tight contact relationship between the elements must be established. An interface element must then be defined between the parts to account for contact, slide and gap between the parts. After assembling and positioning the part, the stiffness in different directions is defined for each element. In this way, the constraining effects such as tack welds or fixturing can be accounted for in each interface. After completion of the weld at each interface, a very high stiffness value should be defined, which corresponds to the tightening of the mating parts [26]. This procedure highly influences the calculation results as shown in Fig. 4.14a and b. In Fig. 4.14a no gap correction was considered and in Fig. 4.14b this was corrected. This Fig. shows how defining a controlled gap between the stiffeners and the skin can reduce out-of-plane distortion. The value of stiffness defined for interface element between the stiffener and the skin controls this out of plane distortion.

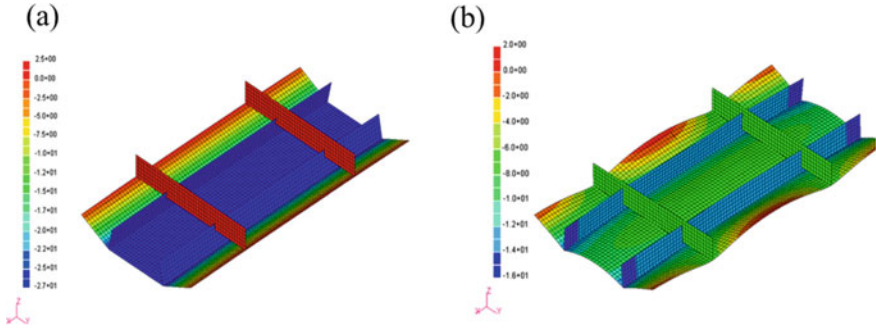


Fig. 4.14 The influence of gap correction in the calculation of distortion by inherent strain method, **a** without gap correction, and **b** with gap correction [26]. Reprinted with permission from Elsevier

4.5 Equivalent Thermal Strain Method

The inherent strain method is only applicable for heating or welding lines which are straight. In curved plates, the introduction of forces caused by inherent strain cannot establish an equilibrium and causes a rigid body movement [30]. The equivalent thermal strain method was effectively used to calculate the welding distortion during welding a pipe [23] and the distortion in other complex structures by inherent strain [30]. The concept of this method originates from the law that states that the equivalent thermal strain is equal to the product of an artificial thermal expansion (α) coefficient and an artificial temperature gradient through the thickness (ΔT) according to:

$$\varepsilon_{th}^{eq} = \alpha \Delta T \tag{4.25}$$

The inherent strain can be directly substituted in the artificial thermal expansion coefficient:

$$\alpha = \varepsilon^* \tag{4.26}$$

The artificial thermal coefficient is zero in areas away from the weld seam in which there is no intrinsic inherent strain. The temperature gradient is defined according to the shape of the inherent strain region around the weld line. This temperature gradient can be obtained by calculating the force and momentum according to two approaches (inherent strain, and equivalent thermal strain methods) and equating the obtained values. The inherent strain in the welding region is almost compressive and asymmetrical across the thickness (Fig. 4.15). The compressive force causes a shrinkage force in the transverse direction and its asymmetry causes a momentum (angular distortion) with respect to the neutral axis (N.A.). This shrinkage force (F) can be calculated by inherent strain value according to:

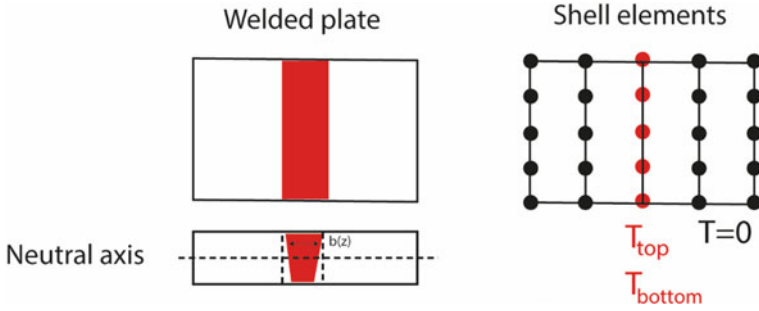


Fig. 4.15 Principle of imaginary node and temperature

$$F = E\varepsilon^* \int b(z)dz \tag{4.27}$$

where $b(z)$ is defined based on the shape of the inherent strain distribution (see Fig. 4.15). The shrinkage force can also be calculated using the equivalent thermal strain method according to:

$$F = E\alpha\Delta Tbh \tag{4.28}$$

where b is the extent of inherent strain and h is the height of it. Similar calculations can be performed for the determination of moment. By equating the forces obtained from both approaches as well as equating the momentum values, the artificial temperature on the top and bottom of the inherent strain region is obtained as:

$$T_{Top} = \frac{1}{A} \int_{-\frac{h}{2}}^{\frac{h}{2}} b(z) \cdot \left(1 - \frac{4}{h} \times z\right) dz \tag{4.29}$$

$$T_{Bottom} = \frac{1}{A} \int_{-\frac{h}{2}}^{\frac{h}{2}} b(z) \cdot \left(1 + \frac{4}{h} \times z\right) dz \tag{4.30}$$

The artificial temperature difference at the top and bottom is responsible for the angular distortion. Further modifications have been applied in the literature [31] to accurately define the artificial temperature and artificial thermal coefficient not only in the transverse direction, but also in the longitudinal one. A trapezoidal shape is mostly used for the inherent strain distribution but other shapes can also be used [30]. The element size is defined by the elements of nodes at which the equivalent forces are applied and is equal to the extent of HAZ [30].

The flowchart of equivalent thermal strain method is depicted in Fig. 4.16. First, a TEP FEM analysis is carried out to calculate the inherent strain in the weld zone.

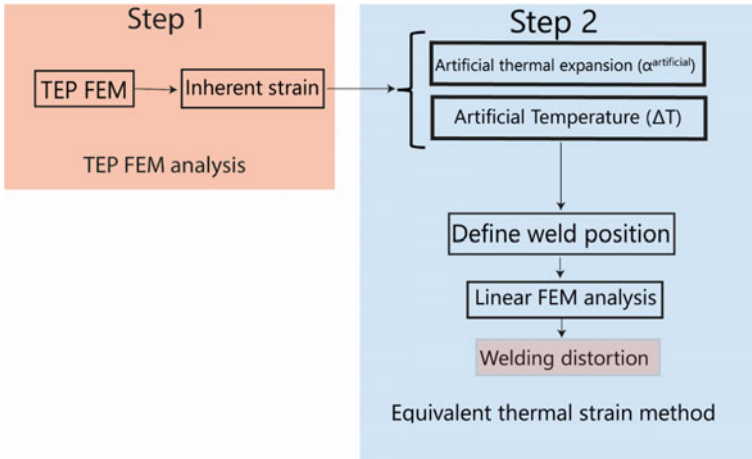


Fig. 4.16 Computation procedure for equivalent thermal strain method

Thereafter, the output of this simulation will be converted to an artificial thermal expansion coefficient and artificial temperature gradient to be used in the linear FEM analysis. The computing time in this procedure is much less than thermal mechanical FEM analysis, as it is a linear FEM. Solving this linear FEM involves two stages, of thermal and mechanical nature. First, the thermal model is solved by linear interpolation taking into account the calculated artificial temperatures. The temperature beyond the inherent strain region is made to be equal to zero. In the second step, the temperature distribution obtained by this thermal FEM analysis is loaded into the mechanical analysis as initial condition. The mechanical model is then solved by considering the artificial thermal expansion coefficient [31]. The value of artificial thermal expansion beyond the inherent strain region is equal to zero. The artificial temperature distribution, as representative of the inherent strain region, determines the bending moment with respect to the neutral axis, as well as the shrinkage level. The transverse distribution of artificial temperature represents the inherent strain component in the transverse direction. The transverse shrinkage and bending are obtained by assigning ϵ_y^* to α .

In addition to the angular and shrinkage distortion, longitudinal distortion can also be modelled by this method, as proposed in [31]. For doing so, the artificial thermal coefficient expansion should be first defined in both the transverse and longitudinal directions. That means that both transverse and longitudinal inherent strains must be calculated after TEP FEM simulation is carried out. However, whether the longitudinal expansion should be considered depends mainly on the structure type and the importance of the calculation of the longitudinal shrinkage.

4.6 Phase Transformation and Materials Properties Effects

The influence of various parameters on the diverse types of residual stress is summarized in Table 4.2. This table shows the effect of the individual parameters which are related to materials conditions, although it does not provide a clear picture of the effects associated to parameter interaction. In addition to the materials properties, variables related to the design of the structure and production can also influence the residual stress [5]. Even minimal changes in the process parameters or the structure dimensions can have a huge influence on the residual stress.

The inclusion of the phase transformation process has a considerable impact on the simulation accuracy since it makes it more representative of the real condition. The phase transformation can induce permanent strain which is called transformation plasticity. The other effect of phase transformation is changing the material properties which has a large effect on residual stress prediction. Figure 4.17 shows the longitudinal and transverse residual stress in the surface of a St37 steel welded with a double V-groove. Microstructural changes occur in the weld zone and HAZ (martensitic transformation) and the differences between the two curves (with and without microstructural change) are noticeable in these regions. In this regard, the proper choice of material properties by considering the phase transformations is critical for the accurate prediction of the residual stress [32]. Usually, phase transformations are predicted in the thermal analysis with the assumption that stress distribution has no effect on the phase transformation [9]. In other words, in the case of simulation problems, it is assumed that the phase transformations are only dependent on the temperature history and the material properties are therefore determined solely in the thermal analysis. The material properties obtained in the thermal analysis are then transferred and used in the mechanical analysis.

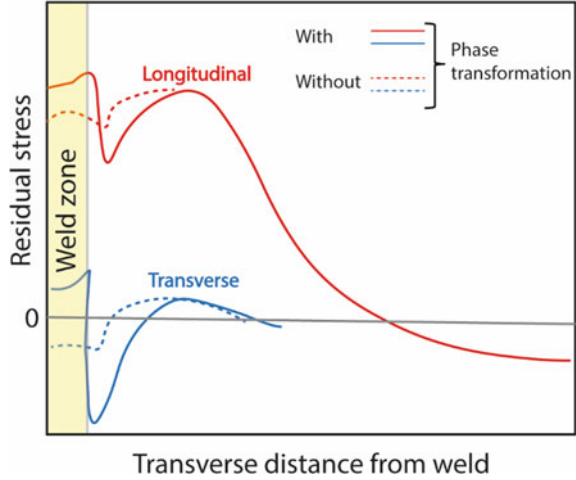
In some cases, it is important to consider the hardening effect in the material in the mechanical analysis. Both kinematic and isotropic hardening have been used to

Table 4.2 Effect of various parameters on different kinds of residual stresses [5]

<i>Shrinkage residual stresses change with:</i>							
$\sigma_{YS} \uparrow$	$d\sigma_{YS}/dT \uparrow$	$\alpha \uparrow$	$E \uparrow$	$\lambda \downarrow$	$dT/dX \uparrow$	$s \downarrow$	$t \uparrow$
<i>Rapid cooling shrinkage residual stresses change with:</i>							
$\sigma_{YS, \Delta T_{\max}} \downarrow$	$\sigma_{YS} - \sigma_{YS, \Delta T_{\max}} \uparrow$	$\alpha \uparrow$	$E \uparrow$	$\lambda \downarrow$	$\Delta T_{\max} \uparrow$	$dT/dt \uparrow$	$t \uparrow$
<i>Phase transformation residual stresses change with:</i>							
$\sigma_{YS, Tu} \uparrow$	$\sigma_{YS, Tu, \min} - \sigma_{YS, Tu, \max} \uparrow$	$\Delta V_{tr} \uparrow$	$E \uparrow$	$\lambda \downarrow$	$M_s \downarrow$	$dT/dt \uparrow$	$s \downarrow$

σ_{YS} is yield stress, $\sigma_{YS, \Delta T_{\max}}$ is yield stress at temperature wherein the temperature difference is maximum, $\sigma_{YS, Tu}$ is yield stress at temperature of phase transformation, α is thermal coefficient, λ is thermal conductivity, E is elastic modulus, s is the width of the seam weld, t is thickness, dT/dt is cooling rate, dT/dX is temperature gradient, M_s is the starting temperature of martensite, ΔV_{tr} is volume change due to phase transformation.

Fig. 4.17 The longitudinal and transverse residual stress in the surface of a St37 steel welded with a double V-groove either with or without considering the phase transformation [33]



calculate the residual stress [18]. With multi-phase welding, the thermal effect of the subsequent layers on the previous layers must be taken into account. In multi-pass welding, a thermal cycle is experienced by each layer which schematically is shown in Fig. 4.18. The thermal history is dependent on several factors such as welding process, material properties, initial or ambient temperature, and the dimension of the weld. When the weld line is long enough, the temperature of each point diminishes to the initial temperature, i.e. the inter-pass temperature is not changing. When the weld line is short there is not enough time between the weld passes for cooling down and the temperature in every point raises after each pass. In these cases, the presence of a thermomechanical cyclic load requires the application of mixed isotropic-kinematic hardening laws in order to take into account both the Bauschinger effect and the cyclic hardening [34]. Figure 4.19 shows these models schematically. Isotropic hardening defines the evolution of the yield stress surface and is obtained from [34]:

$$\sigma^0 = \sigma_0 + Q_{inf} \left(1 - \exp^{-b\dot{\epsilon}_{pl}} \right) \tag{4.31}$$

where σ_0 is the yield stress at zero plastic strain, Q_{inf} and b are material hardening parameters, and $\dot{\epsilon}_{pl}$ is the equivalent plastic strain. The kinematic hardening law is obtained from [34]:

$$\dot{\alpha} = \sum_i \left[C_i \frac{1}{\sigma_0} (\sigma - \alpha) \dot{\epsilon}_{pl} - \gamma_i \alpha \dot{\epsilon}_{pl} \right] \tag{4.32}$$

where $\dot{\alpha}$ is the new yield surface due to kinematic hardening, C_i and γ_i are materials parameter, σ and α are the stress and back stress tensors (determining the translation of the yield surface). A Lemaitre-Chaboche hardening model takes into account both isotropic and kinematic hardening.

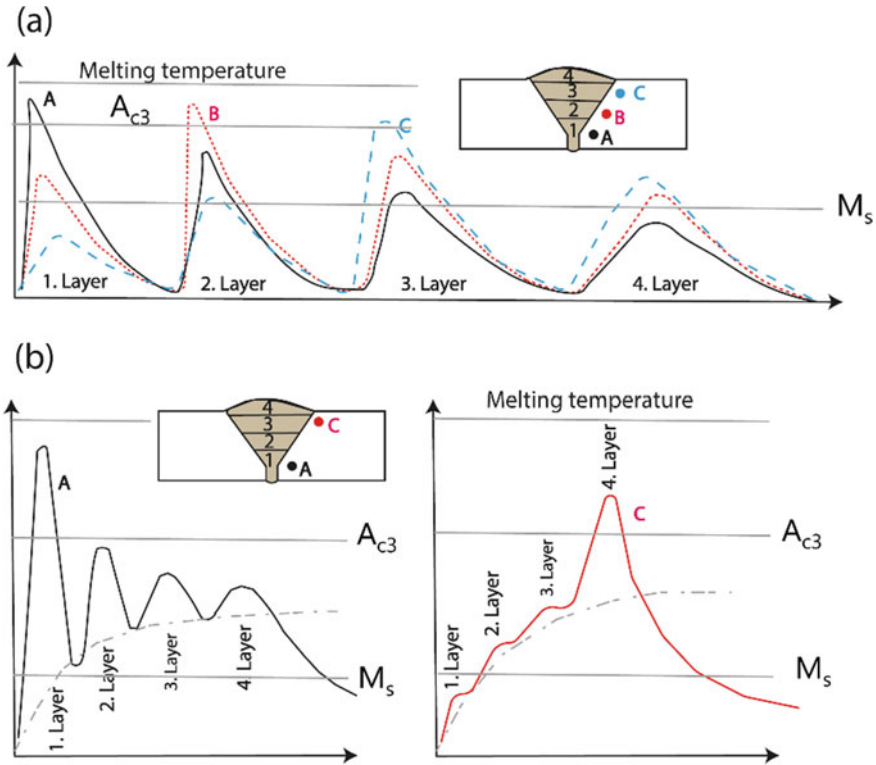
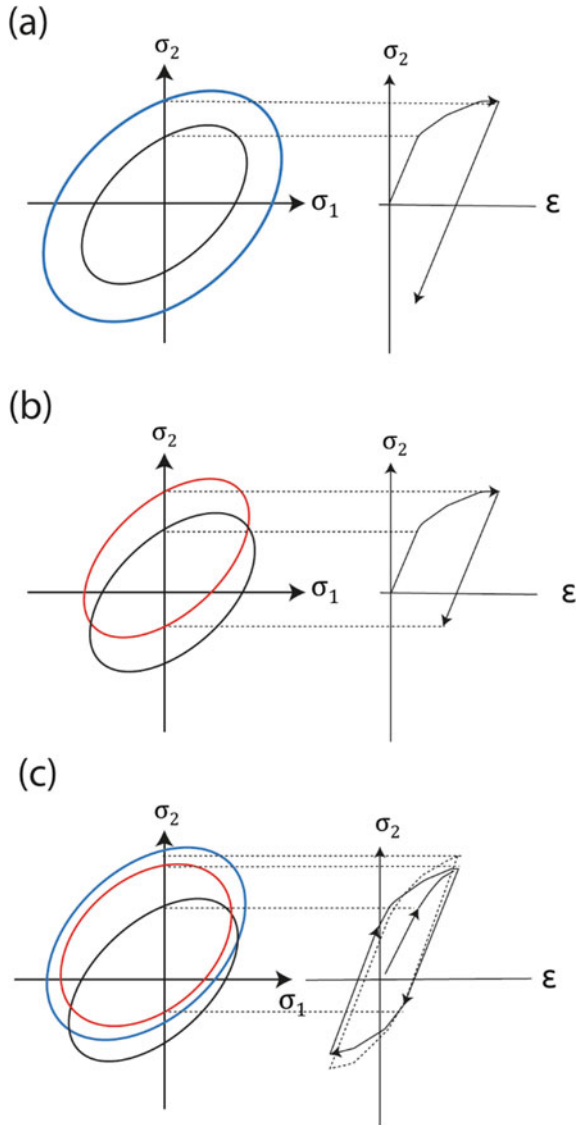


Fig. 4.18 Thermal cycles in some point resulted from multi-pass welding for **a** a long weld line, and **b** a short weld line [35]

In multi-layer welding, creep and annealing effects can occur, which are temperature-dependent phenomena. The former causes stress relief and the latter causes microstructural change. It is reported that taking the annealing effect into account leads to more accurate results than what is achieved by taking into account creep [18]. In fact, during numerical simulation one can generally ignore viscoplastic behavior in cases where there is neither a multi-pass welding nor a stress relief heat treatment. Usually, plastic strain is eliminated by annealing which occurs above a specific annealing temperature and a practical methodology to consider the influence of annealing is to remove any prior strain hardening in a isotropic hardening model in which the yield surface returns to its initial state when the local temperature exceeds the annealing temperature [36]. For example, this temperature for austenitic stainless steel is 1000 °C. In the simulation of a multi-pass welding, considering isotropic hardening, both kinematic hardening and annealing can improve the accuracy of the simulation to predict the residual stress. However, a kinematic hardening model requires several parameters that must be experimentally determined and also leads to larger computational times. It is reported that during the simulation of austenitic stainless steel welding, neglecting kinematic hardening gives a more conservative

Fig. 4.19 Schematic representation of yield surface and stress–strain curve for different material behaviors. **a** Isotropic hardening. **b** Kinematic hardening. **c** Combined isotropic-kinematic hardening [37]. Adopted with permission from Elsevier



result of residual stress magnitude which in engineering applications is desirable [36].

In creep or visco-plastic constitutive models, the in-deformation is time dependent and in stress relieving process creep is almost always present. A creep process has three main stages (primary, secondary and tertiary). When simulating stress relief through creep in the welding, only the second stationary stage should be considered [38]. During a post-weld heat treatment, the process of creep reduces

the residual stresses and can be performed uncoupled with the welding process, i.e. after the completion and cooling of the weld [39]. Norton's law describes well this phenomenon quantitatively [40]:

$$\dot{\varepsilon} = C_1 \sigma^{C_2} e^{-\frac{C_3}{T}} \quad (4.33)$$

where $\dot{\varepsilon}$ is the strain rate, C_1 , C_2 , C_3 are constants of material, 'T' is the temperature, and σ is the stress. The creep effect of reheating in multi-phase welding is mostly neglected in the simulation because creep is a time-dependent phenomenon and the thermal cycles associated to multi-layer welding are too short for creep to play a significant role. Creep is thus only usually considered in the simulation of the post-weld heat treatment which aims mainly to reduce the residual stresses present after welding.

The temperature at which a phase transition occurs (in the solid state) can also strongly influence the level of residual stress. This is especially true for steels in which the HAZ and FZ undergoes austenite phase transformation during heating and the subsequent phase transformation during cooling. The lower the temperature of the phase transition, the greater the reduction in residual stress. In general, phases transformed from austenite during cooling have a higher volume and if the phase transformation from austenite to ferrite occurs at lower temperature, there is necessarily a higher volume expansion because the thermal volume expansion of austenite is higher than that of ferrite. In general, a phase transformation during cooling establishes compressive residual stresses in the weld metal [41] and this residual stress is superimposed on the other stresses caused by rapid cooling (shrinkage stresses). Figure 4.20 shows this phenomenon schematically. The phase transformation and shrinkage all have different effects. Shrinkage causes a tensile stress in longitudinal direction and a compressive stress in transverse direction of the base material. The

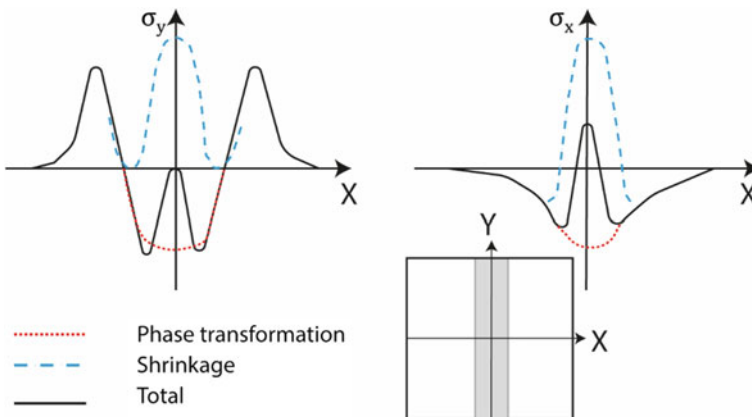


Fig. 4.20 Superposition of shrinkage stress and phase transformation stress in longitudinal and transverse direction [42]

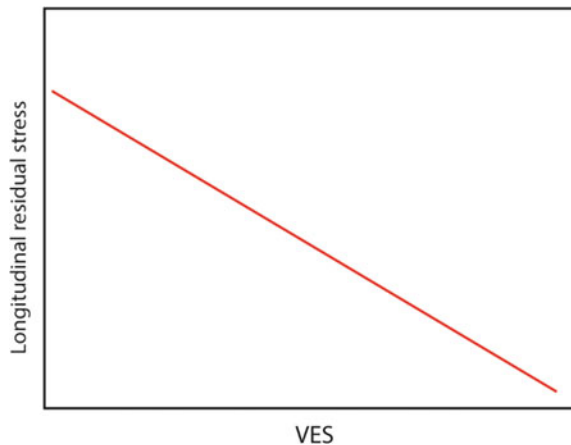
thermal stresses caused by shrinkage are tensile in the weld zone while those caused by phase transformation are mainly compressive. The final shape of the residual stress distribution is then determined by the mechanism which is dominant (transformation, shrinkage, or rapid cooling). Furthermore, other factors such as the number of layers may also influence the stress profile.

In the case of steels which undergo martensitic transformation by cooling, the initial and final temperatures of martensitic transformation (M_s , M_f) as well as the temperature range for martensitic transformation ($M_s - M_f$) have a large effect on the residual stress values [43]. This is due to the volumetric expansion during martensite transformation which compensates for the tensile residual stresses caused by shrinkage and the overall result is a compressive stress on the weld material. Low temperature transformation (LTT) steels are preferable due this. By cooling down to a temperature below the M_s the residual stress level starts to decrease until the temperature reaches M_f . At temperatures lower than M_f the residual stress bounces back and starts to increase. The relationship between the coefficient of thermal expansion (CTE), volume expansion strain (VES) and the temperature range of martensite formation (ΔT) is:

$$CTE = \frac{VES}{\Delta T} \quad (4.34)$$

As the martensite finish temperature in the weld decreases, more residual compressive stress is induced, which is desirable. During a simulation process, the volumetric change due to martensitic transformation can be represented by variation of thermal expansion coefficient with temperature, for two kinds of steels with two different transformation temperatures (LTT1 with $M_s = 245^\circ\text{C}$, $M_f = 100^\circ\text{C}$ and LTT2 with $M_s = 225^\circ\text{C}$, $M_f < 0^\circ\text{C}$). Here, a negative CTE can represent the volume increase due to martensite transformation. The simulation results show that by increasing the VES the compressive residual stress increases, as shown in Fig. 4.21. This also

Fig. 4.21 Relationship between longitudinal residual stress and volume expansion strain (VES)



demonstrates how important it is to choose a filler material with a lower martensite finish temperature (for example LTT2 compared to LTT1), allowing to build up residual compressive stress.

In multi-pass welding, in which LTT materials were used, reheating of each layer by the subsequent layers can enhance the compressive residual stress if the reheat temperature exceeds the austenite transformation. Otherwise, a residual tensile stress would arise in each layer under the influence of the heat of the top layer [44]. This residual stress is very high, driven by the high yield strength of martensite, and can degrade the performance of the component, especially if the HAZ is martensitic as well. An alternative method to reduce residual stress, if the material volume expansion cannot change by martensite formation, is to use a different filler material with a lower yield strength, such as Ni-based filler materials [45]. In this way, although the residual stress adds up during multi-phase welding, it cannot increase in excess because it cannot exceed the nickel's low yield strength.

4.7 Weld Sequence

A fundamental action to reduce the residual stress is to properly design the welding sequence. Generally, a weld path can be sub-divided into a set of partial seams and therefore there are several possible combinations of weld sequences that can be simulated to calculate the resultant residual stress or the distortion level. As the number of sub-welds under consideration increases, so do the possible strategies. If one chooses to divide a path into n sub-welds, the total number of possible combinations would be equal to $2^n \times n!$. For a path with 4 sub-welds there is 384 possible strategies. In the case of spot welding, for an assembly consisting of N_w welds there is $N_w!$ Possible permutations. Running such a large number of simulations is very time-consuming and therefore some specific approaches must be followed to reduce the workload without deteriorating the accuracy of the results. In Chap. 5 some of these approaches are explained.

4.8 Technical Aspects of Residual Stress Simulation

One classical technique used to reduce computational time is to adopt a 2D FE model at the cost of a loss in complexity. In such simplification, a balance should be established between computing time and the detail being captured by the model. Of course, some geometries do not allow for this simplification and require the use of 3D models, such as the case of pipe grith weld in which the residual stresses are rotationally non-symmetric [9]. Another common process is to perform a thermal analysis divided into two main parts: heating and cooling. The results of the thermal history can then be loaded in the mechanical model to predict the residual stresses and distortion. Furthermore, instead of using the results of a moving heat source in

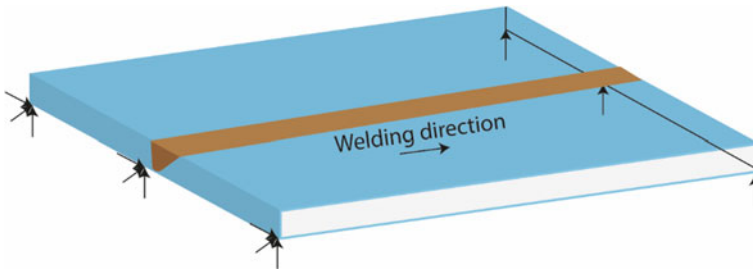


Fig. 4.22 The constraints in simulation of an aluminum alloy welded in butt configuration

the mechanical analysis, an instantaneous heat source can be adopted, although the mesh size is critical for the accuracy of the result [46]. Another strategy that is used to reduce the time it takes a CPU to compute the mechanical model is to limit the load to areas beyond which the heat contribution is negligible [47].

When a filler material is added to the weld, two techniques are utilized to account for the added material [48]: the quiet element (dummy) technique and the element death-rebirth technique. In the dummy technique the elements are active all the time and are initially assigned with dummy material properties. The actual weld material properties are reassigned only after the elements start to cool down. In the element rebirth technique, accurate material properties are initially assigned to elements, but they are inactivated before the corresponding part (the weld material) is deposited. These two techniques are known to be equally effective in large scale problems, with no considerable differences. However, it is advisable to examine the performance of both techniques with regards to the temperature distribution and weld nugget shape.

The constraints on the structures should also be carefully considered. Figure 4.22 shows the constraints in a simulation of an aluminum alloy welded in butt configuration. One edge of the lower surface was fully constrained while the other edge was constrained only along the plate thickness direction. Usually, the out of plane displacement is regarded as the distortion criterion. Constraints play a very important role on the residual stress and the final distortion of the component.

For the determination of accurate results it is necessary to consider the variation of both mechanical and physical properties of material with respect to temperature [49]. The physical properties are considered in thermal analysis and the mechanical properties are considered in mechanical analysis. Figure 4.23 shows an example of variation of materials properties with respect to temperature in a steel.

The element types adopted during the thermal analysis and structural analysis are almost always different. For instance, the literature shows examples where the element types chosen for thermal and mechanical analyses were DC3D20 (a 3D, 20-node quadratic isoparametric element for heat transfer) and C3D8R (a 3D, 8-node linear isoparametric element with reduced integration), respectively [48]. Triangular elements are generally stiff and are not well suited for elastic-plastic analysis. Meshing in a coupled thermo mechanical analysis requires elements that possesses

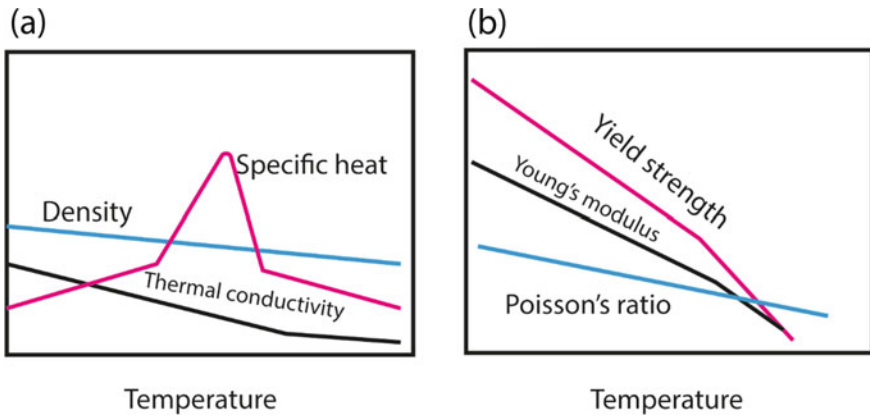


Fig. 4.23 Variation of **a** thermal properties, and **b** mechanical properties of a steel with temperature

both thermal and mechanical degree of freedom. Usually, additional software packages (such as Hypermesh or Femap) are used to mesh complex shapes in order to be further used by simulation software such as Abaqus, Sysweld and so on. Furthermore, in cases where large strains are present, it is fundamental to reduce the step size or mesh size, greatly lengthening the simulation time.

In welding process models, the peak temperature at various locations of the mesh will vary greatly. In the case of steel alloys this causes different microstructures to appear in the HAZ and every microstructure experiences a different thermal strain during cooling. Therefore, a fine mesh is needed in this region in order to take into account these transformations. To reduce computational costs associated to this detailed mesh, a technique named Reduced Geometry can be used which is based on the hypothesis that the temporal and spatial variation of temperature or other parameters is significant only around the welding region [50]. In this regard, only elements in the weld region need to be fine and, in the regions, far from the weld larger elements can be used in order to shorten the simulation time. The finer element size is mandatory to capture the steep gradients of temperature around the weld zone. Furthermore, there is no interest to record the variation of temperature far from the weld zone. Figure 4.24 shows the reduced and standard geometry.

The transient state of welding is decisive on establishment of the steady state condition. The rate of change and the local gradient in transient state are quite high and therefore in the simulation the mesh size and time step must be refined. This lengthens the time of analysis, especially when the metallurgical changes are considered in simulation.

The material characteristics which are needed for the simulation of residual stress are the thermal expansion coefficient, elastic modulus, Poisson's ratio, and yield limit. While the thermal expansion coefficient is temperature dependent, these properties are usually only needed only at low temperatures where the flow stress is high. Simple experiments can be performed to calibrate the simulation and obtain accurate results.

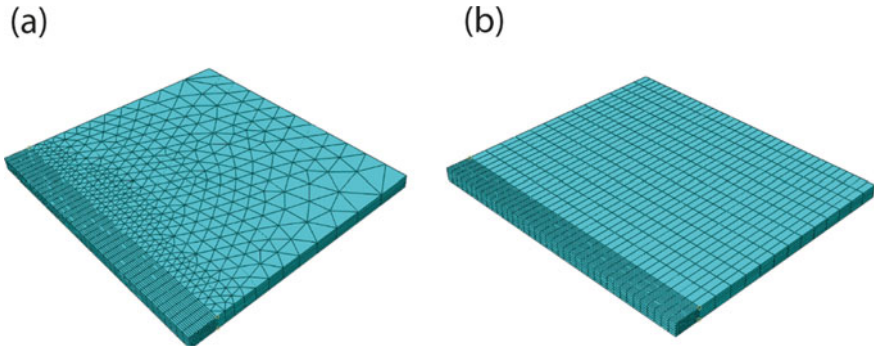


Fig. 4.24 Mesh of the computational model made with **a** reduced geometry, and **b** standard geometry

In this procedure, local properties of the weld in the model are modified and the simulation is repeated until an acceptable match is obtained between the simulation result and the experiment. In industrial applications, the modified properties often do not necessarily closely match the actual properties of the material and changes can be made, for example, to the yield point or other material properties.

References

1. Gong, K., et al.: Effect of dissolved oxygen concentration on stress corrosion cracking behavior of pre-corroded X100 steel base metal and the welded joint in wet–dry cycle conditions. *J. Nat. Gas Sci. Eng.* **77**, 103264 (2020)
2. Javadi, Y., et al.: Investigating the effect of residual stress on hydrogen cracking in multi-pass robotic welding through process compatible non-destructive testing. *J. Manuf. Process.* **63**, 80–87 (2021)
3. Li, L., et al.: Experimental and numerical investigation of effects of residual stress and its release on fatigue strength of typical FPSO-unit welded joint. *Ocean Eng.* **196**, 106858 (2020)
4. Tietz, H.-D.: Grundlagen der Eigenspannungen: Entstehung in Metallen, Hochpolymeren und silikatischen Werkstoffen, Meßtechnik und Bewertung; mit 12 Tab. 1982: Deutscher Verlag für Grundstoffindustrie
5. Hildebrand, J.: *Numerische Schweißsimulation-Bestimmung von Temperatur, Gefüge und Eigenspannung an Schweißverbindungen aus Stahl-und Glaswerkstoffen* (2009)
6. Kannengießer, T.: Untersuchungen zur Entstehung schweißbedingter Spannungen und Verformungen bei variablen Einspannbedingungen im Bauteilschweißversuch. *Shaker* (2000)
7. Hensel, J., Nitschke-Pagel, T., Dilger, K.: On the effects of austenite phase transformation on welding residual stresses in non-load carrying longitudinal welds. *Weld. World* **59**(2), 179–190 (2015)
8. Daichendt, S.: Relaxation strahlbedingter Eigenspannungen unter kombiniert thermisch-mechanischer Beanspruchung in Laserstrahl-Schweißverbindungen einer AlSiMgCu-Knetlegierung. *Universität Bremen* (2011)
9. Mirzaee-Sisan, A., Wu, G.: Residual stress in pipeline girth welds-A review of recent data and modelling. *Int. J. Press. Vessels Pip.* **169**, 142–152 (2019)
10. Radaj, D.: Heat effects of welding: temperature field, residual stress, distortion. *Springer Science & Business Media* (2012)

11. Murakawa, H., Ma, N., Huang, H.: Iterative substructure method employing concept of inherent strain for large-scale welding problems. *Weld. World* **59**(1), 53–63 (2015)
12. Pakkanen, J., Vallant, R., Kičín, M.: Experimental investigation and numerical simulation of resistance spot welding for residual stress evaluation of DP1000 steel. *Weld. World* **60**(3), 393–402 (2016)
13. Lu, Y., et al.: Numerical simulation of residual stresses in aluminum alloy welded joints. *J. Manuf. Process.* **50**, 380–393 (2020)
14. Huang, H., et al.: Toward large-scale simulation of residual stress and distortion in wire and arc additive manufacturing. *Add. Manuf.* **34**, 101248 (2020)
15. Kyaw, P.M., et al.: Numerical study on the effect of residual stresses on stress intensity factor and fatigue life for a surface-cracked T-butt welded joint using numerical influence function method. *Weld. World* **65**(11), 2169–2184 (2021)
16. Ma, N., Umezu, Y.: Application of explicit FEM to welding deformation: analysis. *Weld. Int.: Trans. Worlds Weld. Press* **23**(1), 1–8 (2009)
17. Ikushima, K., Shibahara, M.: Prediction of residual stresses in multi-pass welded joint using idealized explicit FEM accelerated by a GPU. *Comput. Mater. Sci.* **93**, 62–67 (2014)
18. Maekawa, A., et al.: Fast three-dimensional multipass welding simulation using an iterative substructure method. *J. Mater. Process. Technol.* **215**, 30–41 (2015)
19. Tremarin, R.C., Pravia, Z.M.C.: Analysis of the influence of residual stress on fatigue life of welded joints. *Latin Am. J. Solids Struct.* **17** (2020)
20. Islam, M., et al.: Simulation-based numerical optimization of arc welding process for reduced distortion in welded structures. *Finite Elem. Anal. Des.* **84**, 54–64 (2014)
21. Radaj, D.: *Eigenspannungen und Verzug beim Schweißen: Rechen- und Messverfahren*, Fachbuchreihe Schweißtechnik, vol. 143. Verlag für Schweißen und Verwandte Verfahren, DVS-Verlag, Düsseldorf (2002)
22. Murakawa, H., Deng, D., Ma, N.: Concept of inherent strain, inherent stress, inherent deformation and inherent force for prediction of welding distortion and residual stress. *Trans. JWRI* **39**(2), 103–105 (2010)
23. Wu, C., Wang, C., Kim, J.-W.: Welding distortion prediction for multi-seam welded pipe structures using equivalent thermal strain method. *J. Weld. Join.* **39**(4), 435–444 (2021)
24. Honaryar, A., et al.: Numerical and experimental investigations of outside corner joints welding deformation of an aluminum autonomous catamaran vehicle by inherent strain/deformation FE analysis. *Ocean Eng.* **200**, 106976 (2020)
25. Wang, J., et al.: Numerical prediction and mitigation of out-of-plane welding distortion in ship panel structure by elastic FE analysis. *Mar. Struct.* **34**, 135–155 (2013)
26. Murakawa, H., et al.: Applications of inherent strain and interface element to simulation of welding deformation in thin plate structures. *Comput. Mater. Sci.* **51**(1), 43–52 (2012)
27. Kim, T.-J., Jang, B.-S., Kang, S.-W.: Welding deformation analysis based on improved equivalent strain method considering the effect of temperature gradients. *Int. J. Naval Archit. Ocean Eng.* **7**(1), 157–173 (2015)
28. Yi, B., Wang, J.: Mechanism clarification of mitigating welding induced buckling by transient thermal tensioning based on inherent strain theory. *J. Manuf. Process.* **68**, 1280–1294 (2021)
29. Ma, N., et al.: Inherent strain method for residual stress measurement and welding distortion prediction. In *International Conference on Offshore Mechanics and Arctic Engineering*. American Society of Mechanical Engineers (2016)
30. Ha, Y.S., Cho, S.H., Jang, T.W.: Development of welding distortion analysis method using residual strain as boundary condition. In *Materials Science Forum*. Trans Tech Publ. (2008)
31. Wu, C., Kim, J.-W.: Numerical prediction of deformation in thin-plate welded joints using equivalent thermal strain method. *Thin-Walled Struct.* **157**, 107033 (2020)
32. Smith, M.C., Smith, A.C.: Advances in weld residual stress prediction: a review of the NeTTG4 simulation round robins part 2, mechanical analyses. *Int. J. Press. Vessels Pip.* **164**, 130–165 (2018)
33. Argyris, J., Szimmat, J.: Finite element analysis of arc-welding processes. In: *International Conference on Numerical Methods in Problems*, vol. 3 (1983)

34. Muránsky, O., et al.: Numerical analysis of retained residual stresses in C(T) specimen extracted from a multi-pass austenitic weld and their effect on crack growth. *Eng. Fract. Mech.* **126**, 40–53 (2014)
35. Rykalin, N., Fritzsche, C.: *Berechnung der wärmevorgänge beim schweissen: aus dem Russ.* Verlag Technik (1957)
36. Deng, D., et al.: Influence of material model on prediction accuracy of welding residual stress in an austenitic stainless steel multi-pass butt-welded joint. *J. Mater. Eng. Perform.* **26**(4), 1494–1505 (2017)
37. Teimouri, R., Amini, S., Guagliano, M.: Analytical modeling of ultrasonic surface burnishing process: evaluation of residual stress field distribution and strip deflection. *Mater. Sci. Eng., A* **747**, 208–224 (2019)
38. Ren, S., et al.: Finite element analysis of residual stress in 2.25 Cr-1Mo steel pipe during welding and heat treatment process. *J. Manuf. Proc.* **47**:110–118 (2019)
39. Deshpande, A.A., et al.: Combined butt joint welding and post weld heat treatment simulation using SYSWELD and ABAQUS. *Proc. Instit. Mech. Eng. Part L: J. Mater.: Des. Appl.* **225**(1), 1–10 (2011)
40. Tan, L., Zhang, J.: Effect of pass increasing on interpass stress evolution in nuclear rotor pipes. *Sci. Technol. Weld. Joining* **21**(7), 585–591 (2016)
41. Neubert, S.: *Simulationsgestützte Einflussanalyse der Eigenspannungs- und Verzugsausbildung beim Schweißen mit artgleichen und nichtartgleichen Zusatzwerkstoffen.* Technische Universität Berlin (Germany) (2018)
42. Wohlfahrt, H., Nitschke-Pagel, T., Kaßner, M.: Schweißbedingte Eigenspannungen-Entstehung und Erfassung. Auswirkung und Bewertung. *DVS BERICHT* **187**, 6–13 (1997)
43. Feng, Z., et al.: Transformation temperatures, mechanical properties and residual stress of two low-transformation-temperature weld metals. *Sci. Technol. Weld. Join.* **26**(2), 144–152 (2021)
44. Feng, Z., et al.: Investigation of the residual stress in a multi-pass T-welded joint using low transformation temperature welding wire. *Materials* **14**(2), 325 (2021)
45. Guo, Q., et al.: Influence of filler metal on residual stress in multi-pass repair welding of thick P91 steel pipe. *Int. J. Adv. Manuf. Technol.* **110**(11), 2977–2989 (2020)
46. Pu, X., et al.: Simulating welding residual stress and deformation in a multi-pass butt-welded joint considering balance between computing time and prediction accuracy. *Int. J. Adv. Manuf. Technol.* **93**(5), 2215–2226 (2017)
47. Tchoumi, T., Peyraut, F., Bolot, R.: Influence of the welding speed on the distortion of thin stainless steel plates—Numerical and experimental investigations in the framework of the food industry machines. *J. Mater. Process. Technol.* **229**, 216–229 (2016)
48. Ahn, J., et al.: Determination of residual stresses in fibre laser welded AA2024-T3 T-joints by numerical simulation and neutron diffraction. *Mater. Sci. Eng., A* **712**, 685–703 (2018)
49. Yu, H., et al.: Numerical simulation optimization for laser welding parameter of 5A90 Al-Li alloy and its experiment verification. *J. Adhes. Sci. Technol.* **33**(2), 137–155 (2019)
50. Farias, R., Teixeira, P., Vilarinho, L.: An efficient computational approach for heat source optimization in numerical simulations of arc welding processes. *J. Constr. Steel Res.* **176**, 106382 (2021)